Accelerated convergence of convective simulations using boundary value problems

Evan H. Anders and Benjamin P. Brown
Dept. Astrophysical & Planetary Sciences, University of Colorado – Boulder, Boulder, CO 80309, USA and Laboratory for Atmospheric and Space Physics, Boulder, CO 80303, USA

Jeffrey S. Oishi
Department of Physics and Astronomy, Bates College, Lewiston, ME 04240, USA

We present a method for using coupling Boundary value problems (BVPs) with Initial value problems (IVPs) in order to achieve thermally converged convective solutions on dynamical timescales, rather than the long thermal timescale. We demonstrate the similarity between the solution reached via BVP and the solution reached by a long thermal rundown of the IVP, and demonstrate that this method works at a large range of supercriticalities. We use this method to achieve converged solutions at high Ra, and discuss its extension to more complex scenarios, such as stratified, compressible convection.

I. INTRODUCTION

Natural convection occurs in the presence of disparate timescales. Granules on the solar surface overturn on the order of 10 minutes, whereas deep motions in the Sun are likely at low Mach number and constrained by the solar rotation rate of ∼1 month. Both of these dynamical timescales are vastly shorter than the Sun's average timescale of energy transport, which is the Kelvin-Helmholtz timescale of nearly 3×10^7 *years* [1]. As simulations aim to model natural convection by increasing into the high-Rayleigh Number (Ra) regime, where diffusive timescales are much longer than dynamical timescales [2], achieving converged simulations will require runs which span a greater number of convective timescales in order to thermally converge. Furthermore, with increasing Ra and decreasing diffusivities, motions become more turbulent and require finer grid meshes and shorter timesteps to resolve turbulent motions, increasing the simulation time required for each overturn timescale. These two effects conspire to make achieving thermally converged, high-Ra, astrophysically interesting simulations an intractable problem using modern numerical tools.

Prior studies of stratified convection in which a convective layer lies between stable layers have used the knowledge of Mixing Length Theory (MLT) to adjust the initial thermodynamic structure of the atmosphere to a state which is closer to the adiabat chosen by convection [3]. However, most studies of convection do not contain stable layers above and below the convection zone, and the presence of hard boundaries and the boundary layers that they form make it difficult to know the correct evolved adiabat *a priori*.

Here we present a method for using simple boundary value problems (BVPs), along with information about the evolved flow fields, to fast-forward the slow thermal evolution of convecting simulations. We run two sets of experiments: one in which we allow convective simulations to evolve for a full thermal timescale before taking measurements, and another in which we employ a fast-forwarding, BVP technique which occurs on dynamical timescales. We compare these two sets of simulations to show the validity of the BVP technique. Then, we use the BVP technique to run simulations at high Ra, in the regime where running for thermal timescales becomes computationally intractable.

II. EXPERIMENT

We adopt the Oberbeck-Boussinesq approximation. Under this choice, the fluid has constant kinematic viscosity (ν), thermal diffusivity (κ), and coefficient of thermal expansion (α). The variables of the fluid that are evolved are the velocity, $\boldsymbol{u} = u\hat{x} + v\hat{y} + w\hat{z}$, the temperature $T = T_0 + T_1$, and the pressure. The density of the fluid is a constant ρ_0, except on the term where the constant gravitational acceleration, $\boldsymbol{g} = -g\hat{z}$ acts in the vertical momentum equation, in which case it is $\rho = \rho_0(1 - \alpha T_1)$. Under these choices, the equations of motion are [4]

$$\nabla \cdot \boldsymbol{u} = 0, \tag{1}$$

$$\frac{\partial \boldsymbol{u}}{\partial t} + \boldsymbol{u} \cdot \nabla \boldsymbol{u} = -\frac{1}{\rho_0}\nabla P - g(1 - \alpha T_1)\hat{z} + \nu \nabla^2 \boldsymbol{u}, \tag{2}$$

$$\frac{\partial T_1}{\partial t} + \boldsymbol{u} \cdot \nabla (T_0 + T_1) = \kappa \nabla^2 T_1, \tag{3}$$

We non-dimensionalize these equations such that length scales are in units of the layer height (L_z), temperature is in units of the initial temperature jump across the layer ($\Delta T_0 = L_z \nabla T_0$), and time is in units of the freefall timescale ($L_z/v_{\rm ff}$), where the freefall velocity is $v_{\rm ff} = \sqrt{\alpha g L_z^2 \nabla T_0}$. We further re-arrange the momentum equation by introducing a reduced pressure $\varpi \equiv P/\rho_0 + \phi + |\boldsymbol{u}|^2/2$, where $\boldsymbol{g} = -\nabla\phi$ is the gravitational potential. Despite containing a nonlinear $\boldsymbol{u}$ component, the nature of P in Rayleigh-Bénard convection, as a (whatever it's called) allows us to treat ϖ as a linear unknown, without a need to resolve its different components. We time evolve the equations in the form,

$$\nabla \cdot \boldsymbol{u} = 0, \tag{4}$$

$$\frac{\partial \boldsymbol{u}}{\partial t} + \nabla\varpi - T_1\hat{z} + \mathcal{R}\nabla\times\boldsymbol{\omega} = \boldsymbol{u}\times\boldsymbol{\omega} \tag{5}$$

$$\frac{\partial T_1}{\partial t} - \mathcal{P}\nabla^2 T_1 + w\frac{\partial T_0}{\partial z} = -\boldsymbol{u}\cdot\nabla T_1, \tag{6}$$

where $\boldsymbol{\omega} = \nabla\times\boldsymbol{u}$ is the vorticity. We find this form of the momentum equation to be slightly faster numerically than the standard form in Eq. (2). The dimensionless control parameters are set by the Rayleigh and Prandtl numbers,

$$\mathcal{R} \equiv \sqrt{\frac{\rm Pr}{\rm Ra}}, \qquad \mathcal{P} \equiv \frac{1}{\sqrt{\rm Pr\,Ra}}, \qquad {\rm Ra} = \frac{g\alpha L_z^4 \nabla T_0}{\nu\chi} = \frac{(L_z\, v_{\rm ff})^2}{\nu\chi}, \qquad {\rm Pr} = \frac{\nu}{\chi}. \tag{7}$$

The dimensionless vertical extent of the domain is $z = [-1/2, 1/2]$, and at the boundaries we impose no-slip, impenetrable boundary conditions such that $w = u = v = 0$ at $z = \pm 1/2$. At the lower boundary, we employ a fixed flux condition such that $\partial T_1/\partial z = 0$ at $z = -1/2$, and we impose a fixed temperature condition $T_1 = 0$ at $z = 1/2$. Both horizontal directions are periodic, extending over a range $x, y = [0, \Gamma]$, where the aspect ratio is $\Gamma = 2$.

The chosen thermal boundary conditions at the upper and lower plates determine key quantities of the evolved state. Studies of incompressible, Boussinesq, Rayleigh-Bénard convection often employ fixed temperature (Dirichlet) or fixed heat flux (Neumann) boundary conditions at both plates. Dirichlet conditions represent plates of infinite conductivity, whereas Neumann conditions model plates of finite conductivity. In both cases, choosing symmetric boundary conditions maintains overall system symmetry, and despite evolving towards different thermal structures, both types of conditions transport heat in the same manner [5]. Studies of convection which aim to model astrophysical systems such as stars often employ a mixture of these two types of boundary conditions [6–8]. The flux at the lower boundary is fixed, modeling the constant energy generation of the stellar core, while the outer boundary condition is held at a fixed temperature, modeling the surface of a star which must output the energy generated internally. This setup is a useful model for understanding natural systems, but simulations which employ these boundary conditions suffer from a long thermal relaxation as the atmosphere loses energy and approaches the adiabat chosen by the Dirichlet condition. We choose these conditions in part to better understand them, and in part because these conditions minimize the number of assumptions that must be made in setting up the boundary value problem.

A. The Boundary Value Problem

It is a reasonable assumption to naively guess that convection will evolve the mean temperature profile that drives it over the course of a thermal diffusion time, $t_\chi \approx \mathcal{P}^{-1}$. Thus, as Ra increases, the timescale for achieving a thermally converged mean temperature profile becomes intractable. This prohibitively long thermal timescale in a Direct Numerical Simulation (DNS) can be skipped by coupling the DNS with a simple Boundary Value Problem (BVP) solve. By using information about the evolved dynamical state of the atmosphere, a BVP can be used to solve for the evolved atmospheric state on short timescales. A comparison of a simulation running for the thermal timescale, and another where a BVP is used to fast-forward atmospheric evolution, are shown in Fig 1a&b.

The Boussinesq BVP in essence contains equations of hydrostatic balance and thermal equilibrium,

$$\frac{\partial}{\partial z}\left\langle\varpi\right\rangle - \left\langle T_1\right\rangle\hat{z} = \left\langle\boldsymbol{u}\times\boldsymbol{\omega}\right\rangle, \tag{8}$$

$$\frac{\partial}{\partial z}\left\langle wT_1\right\rangle - \frac{1}{\rm PrRa}\frac{\partial^2}{\partial z^2}\left\langle T_1\right\rangle = 0, \tag{9}$$

where $\langle A\rangle$ represents a time- and horizontally averaged profile of the quantity A. These equations arise from assuming that the atmosphere is in a steady state ($\partial_t \to 0$), then taking time and horizontal averages of Eqns (5&6) and neglecting terms that vanish due to the symmetry of the problem. Convective flows are perturbations around a thermal profile defined by these equations in the proper evolved, statistically stationary state.

Under eqns (8&9), the thermal structure ($\langle T_1\rangle$, $\langle\varpi\rangle$) of the atmosphere is fully determined by the specification of two profiles: the convective flux, $F_{conv} = \langle wT_1\rangle$, and the nonlinear advection, $\langle\boldsymbol{u}\times\boldsymbol{\omega}\rangle$. If these profiles are known, then solving for $\langle T_1\rangle$ and $\langle\varpi\rangle$ depends only upon the choice of boundary conditions.

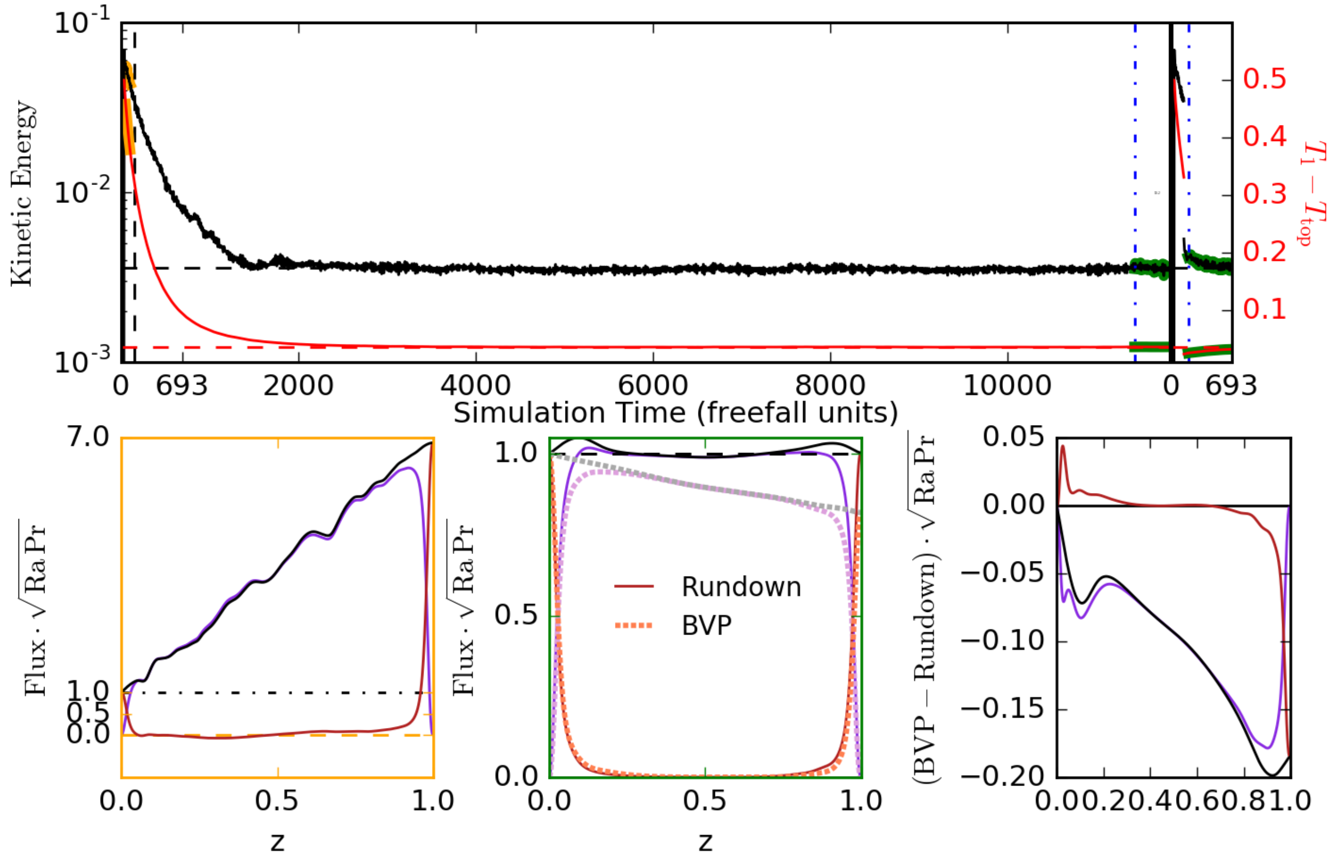

FIG. 1. Traces of system energies vs. time for a long thermal rundown (a) and BVP convergence (b) are shown for Ra = $1.30 \cdot 10^8$ ($S = 10^5$). The horizontal extent of the subplots is set such that one simulation time unit takes up an equal amount of paper space in (a) and (b). The dashed vertical line on (a) represents the time at which the BVP is solved on the run in (b), and the horizontal dashed lines show the equilibrium value of the energies. (c) System fluxes early in the run (the orange highlights in (a)). Black is the sum of the flux, purple is the convective flux, and red is the conductive flux. (d) Fluxes in the converged rundown IVP compared to the "converged" BVP. The sum of flux is shown in black & grey, the convective flux is shown in purple & pink, and the conductive flux is shown in red & orange. (e) The differences between the BVP and rundown fluxes is shown. While not in perfect agreement, the BVP fluxes are much closer to the converged state than the initial fluxes, as in (c).

By definition, the profile of F_{conv} is not in its time stationary early in the DNS. In fact, as the atmosphere approaches the isotherm specified by the upper (fixed T) boundary condition, the motions display an asymmetric flux as energy leaks through the upper boundary condition (Fig. 1c) in order to reach a lower temperature state. In order to construct the evolved convective flux from the current fluxes in the atmosphere, we assume that the atmospheric dynamics have properly developed the thickness of the boundary layers, or that the quantities

$$f_{\text{conv}} = \frac{F_{\text{conv}}}{F_{\text{tot}}} \qquad f_{\text{cond}} = \frac{F_{\text{cond}}}{F_{\text{tot}}} \tag{10}$$

early in the evolution are the same as those in the final steady state solution. By definition, the evolved total flux through the atmosphere must be the same as the flux entering the atmosphere at the bottom boundary, $F_{\text{tot, steady}} = F_{\text{bot}}$. The proper enthalpy flux profile to feed in to Eqn. (9) is then $\langle wT_1\rangle_{\text{steady}} = F_{\text{tot, steady}} \cdot f_{\text{conv}}$. Presumably, over the course of the simulation, the velocity field and temperature fluctuations naturally scale like $d(z) = \langle wT_1\rangle_{\text{steady}} / \langle wT_1\rangle$, and so it is necessary to multiply the velocity field and the fluctuations around the mean in T_1 by $\sqrt{d}$. This also means that $\langle \boldsymbol{u} \times \boldsymbol{\omega}\rangle_{\text{steady}} = d\,\langle \boldsymbol{u} \times \boldsymbol{\omega}\rangle$. Once these profiles are appropriately adjusted, they can be used in the BVP solve to find the mean profiles of T and ϖ.

In general, the BVP solve is completed in the following steps:

1. Run the convective DNS. Once the convection achieves a volume-averaged Re of $\sqrt{\text{Ra}/\text{Ra}_{\text{crit}}}$, wait for 50 time units. Then, start taking the averages of F_{conv} and F_{tot}, waiting either 30 time units or until the profiles are

converged to 1 part in 1000, whichever is a more difficult. This ensures that the profiles being used in the BVP are steady and smooth, and that they sample the full behavior of the convection.

2. Construct $\langle wT_1 \rangle_{\text{steady}}$ and $\langle \boldsymbol{u} \times \boldsymbol{\omega} \rangle_{\text{steady}}$ from the flux profiles.

3. Solve for $\langle T_1 \rangle$ and $\langle \varpi \rangle$ of the evolved state. Adjust the mean profiles in the IVP.

4. Multiply the velocity field and the fluctuations in T_1 about its horizontal average by $\sqrt{d}$ in the IVP.

5. Continue running the IVP for 50 time units to allow for the velocities to equilibrate to their new background state.

B. Numerics

We utilize the Dedalus[1] pseudospectral framework [9] to time-evolve (4)-(6) using an implicit-explicit (IMEX), third-order, four-step Runge-Kutta timestepping scheme RK443 [10]. The temperature field is decomposed as $T = T_0(z) + T_1(x, y, z, t)$ and the velocity is $\boldsymbol{u} = w\hat{\boldsymbol{z}} + u\hat{\boldsymbol{x}} + v\hat{\boldsymbol{y}}$. In our 2D runs, $v = 0$. Variables are time-evolved on a dealiased Chebyshev (vertical) and Fourier (horizontal, periodic) domain in which the physical grid dimensions are 3/2 the size of the coefficient grid. Domain sizes range from 32x128 coefficients at the lowest values of Ra to 1024x4096 coefficients at $\text{Ra} > 10^9$ in 2D.

As initial conditions, we fill T_1 with random white noise whose magnitude is $10^{-6}(\text{Ra Pr})^{-1/2}$. This ensures that the initial perturbations are much smaller than the evolved convective temperature perturbations, even at large Ra. We filter this noise spectrum in coefficient space, such that only the lower 25% of the coefficients have power.

In 2D, there are often multiple steady state solutions (e.g., 2-roll and 3-roll solutions) which have slightly different flow properties (heat transport, etc.). Even though the initial perturbations are very small, they shape the convective transient and thus determine the nature of the steady state convection, at least in the laminar regime. In order to ensure that our results are not biased by differences in flow structure, we ran the simulations using distinct random temperature perturbations so as to compare statistics in comparable flow fields. In 3D, rolls are nonstationary over convective timescales, and so these effects need not be considered there.

III. RESULTS

While the differences in the fluxes in Fig. 1 are small, it is important to determine if the velocity fluctuations and point-by-point nonlinear transport are the same in the evolved state. Fig. 2 overlays the probability distribution functions of the vertical and horizontal velocities, as well as the fully nonlinear portion of the convective flux for the same case as is shown in Fig. 1. The PDFs are quite similar visually, and have a similarity of (XYZ) according to a Kolmogorov-Smirnov statistic.

In addition to getting the nonlinear dynamics mostly correct, we show that the BVP method retrieves the proper temperature profile, see e.g., Fig. 3. Here the BVP profile retrieves the mean profile of the temperature to within 1% accuracy, and temperature fluctuations in the two runs have a similarity of (XYZ) according to a Kolmogorov-Smirnov statistic.

This method works across a broad range of supercriticality. In Fig. 4, we show measurements of the volume-averaged Nusselt number, Reynolds number, and temperature. We use standard definitions of the Nusselt number and Reynolds numbers,

$$\text{Nu} = \frac{\left\langle wT - (\text{Ra Pr})^{-1/2}\nabla T \right\rangle}{\left\langle -(\text{Ra Pr})^{-1/2}\nabla T \right\rangle} = 1 + \frac{\langle wT \rangle}{-\Delta T}\sqrt{\text{Ra Pr}}, \qquad \text{Re} = \frac{|\boldsymbol{u}| L_z}{\nu}, \tag{11}$$

where $\Delta T = T(z = 1/2) - T(z = -1/2)$ is the evolved temperature difference between the top and bottom plates. This form of the Nusselt number is valid even when the system is not yet in flux equilibrium, and reduces to the standard fixed flux definition of $\text{Nu} = [1 - \langle wT \rangle / P]^{-1}$ [5]. We find a scaling law of $\text{Nu} \propto \text{Ra}^{2/3}$, much steeper than a standard 2/7 or 1/3 scaling law [5]. Furthermore, we find that $\text{Re} \propto \text{Ra}^{0.425}$. The average temperature approaches the value at the top of the domain as Ra increases.

[1] http://dedalus-project.org/

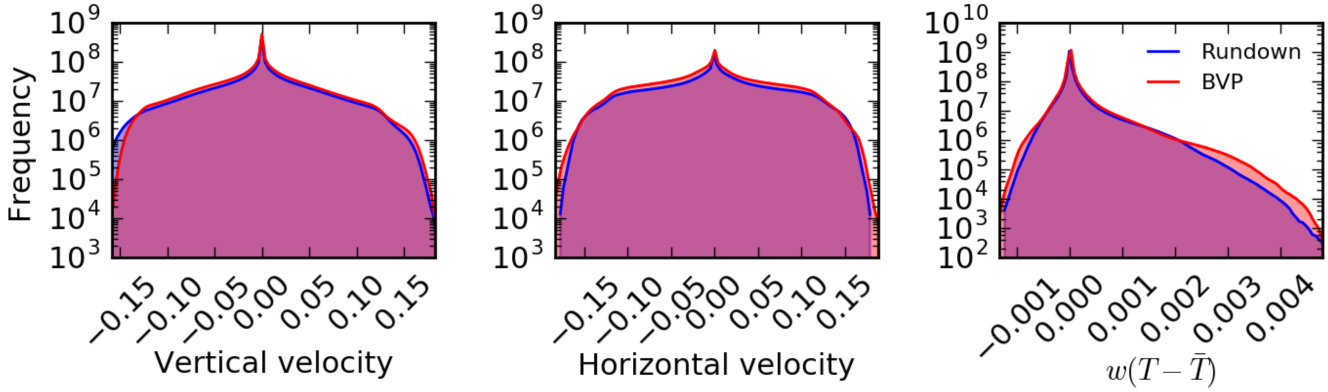

FIG. 2. Frequency distribution functions of the vertical velocity (a), horizontal velocity (b), and nonlinear vertical transport (c) are shown for a 2D run at $S = 10^5$. We sample flows every 0.1 time units for 500 freefall times, and include the flows at all points on the grid at each of these samples in these distributions. All distributions are biased by the no-slip, impenetrable boundary conditions, coupled with the dense spacing of our Chebyshev grids near the boundaries, so there is a large peak around zero. The distributions, and thus the nonlinear dynamics, are broadly similar, but they do not pass a two-tailed Kolmogorov-Smirnov similarity test. (NOTE TO CO-AUTHORS: I NEED TO THINK BETTER ON HOW TO COMPARE PDFS, IF YOU HAVE IDEAS PLEASE SEND THEM)

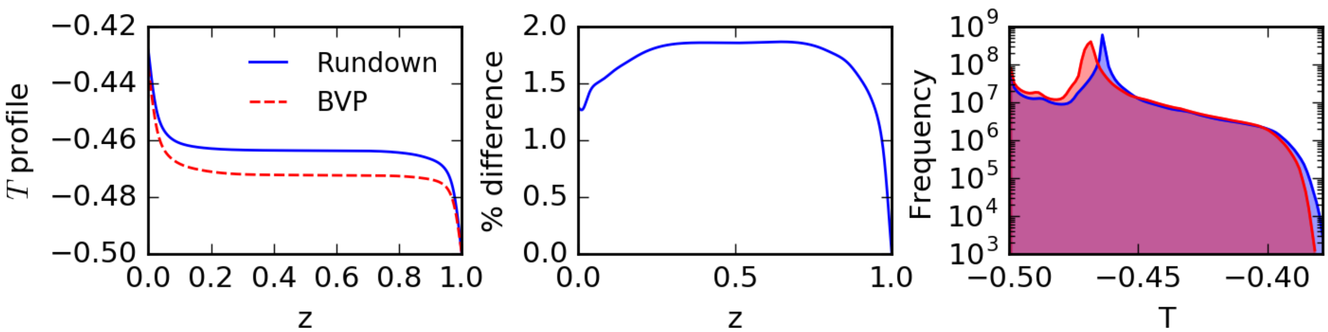

FIG. 3. Comparisons of the evolved thermodynamic states of a BVP solution and a long IVP rundown at $S = 10^5$ are shown. (a) Evolved temperature profiles, as a function of height. (b) The percentage difference between the temperature profiles (as shown in (a)), as a function of height. (c) Frequency distributions, as in Fig. 2, comparing the values of the point-by-point temperatures over the averaging window. The mode of the frequency distribution has a distinct offset between the two runs due to the clear difference between the profiles in (a), but the thermal fluctuations about the mean which drive the convection are similar (AS IN FIG. 2, I NEED TO THINK MORE ON THE PDF COMPARISON).

The final morphology of the flows is very important in determining the exact value of Nu and Re. In general, a two-roll state vs. a three-roll state will have entirely different statistics – different Nu, Re, and average temprature (and as a result, different size boundary layers). Thus, in 2D studies, it is essential to study flows of a similar morphology in order to see a clear trend.

IV. DISCUSSION & CONCLUSIONS

While imperfect, the method presented here is a first step towards taking meaningful measurements of highly turbulent convection on manageable, human timescales. As demonstrated in Figs. 1-4, this BVP method quickly converges simulations to within a few percent of the true final state, while preserving the natural behavior of the convective solution (such as the oscillatory nature of high-Ra 2D states in 4).

While not perfect, the BVP method here has one major benefit over some of the other methods currently being used to achieve high Ra solutions. One oft-used method is that of bootstrapping, in which the converged solution of a low-Ra state is used as initial conditions for a higher-Ra simulation. While these methods are extremely powerful,

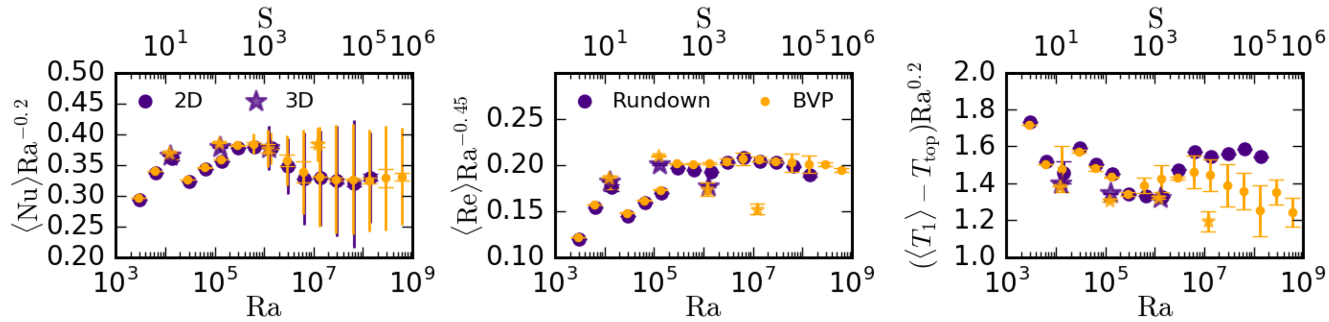

FIG. 4. Compensated scaling plots are shown for the Nusselt number (a), the Reynolds number (b), and the volume-averaged temperature (c). All plots are linear(y)-log(x), and any differences vertically are generally small. Symbols represent the mean value of a measurement, vertical lines represent the standard deviation of the measurement over the time window, and error bars represent the shift in the mean value over the window. (a) Nu, which measures heat transport, scales roughly like $Ra^{1/5}$, and above Ra$\geq 10^6$, simulations display horizontally oscillating plumes which have oscillating periods of high transport and low transport. The mean value is marginally diminished as a result, and the range of Nu over time is large. (b) Re, which measures the level of turbulence in the evolved solution, scales as $\mathrm{Ra}^{0.45}$ in 2D and (something else) in 3D. (c) The average temperature flucutation, minus the top temperature, gives us a measure of the extent of the upper boundary, and is in some ways a more stationary proxy for Nu, and it displays similar scaling. The temperature profile is slow to adjust, and differences between BVP solutions and rundown solutions are easier to pick out.

they are influenced by hysteresis effects, and the powerful, steady rolls achieved at low Ra can result in an artifically over-stable high-Ra roll solution. The BVP method can be used with random noise initial conditions which allow the convective solution to be naturally chosen by the dynamics.

One benefit of the method presented here is that it can be easily extended to more complicated configurations. For example, to use this method in simulations of stratified compressible convection, one need only adapt the BVP equations to the appropriate equations of hydrostatic equilibrium, $\nabla P = -\rho \boldsymbol{g}$, and thermal equilibrium, $\nabla \cdot (F_{\mathrm{cond}} + F_{\mathrm{conv}}) =$ sources, for the problem at hand. In compressible convection, where the density is allowed to change, one must also use the knowledge of stellar structure codes and add an equation of mass conservation in order to ensure that the BVP does not spuriously add or remove mass from the system.

This method can be extended to other boundary conditions, as well. To solve for fixed temperature boundary conditions, the difficulty is in finding the amount of flux through the system – but this can be done by using the ratios f_{conv} and f_{cond}. In the case of fixed flux boundary conditions, there is degeneracy in the temperature solution which can come out of the BVP, but in using knowledge about the system – such as the initial symmetry of the RB state around $T_1 = 0$, the final solution can be pegged onto the proper profile.

ACKNOWLEDGMENTS

EHA acknowledges the support of the University of Colorado's George Ellery Hale Graduate Student Fellowship. This work was additionally supported by NASA LWS grant number NNX16AC92G. Computations were conducted with support by the NASA High End Computing (HEC) Program through the NASA Advanced Supercomputing (NAS) Division at Ames Research Center on Pleiades with allocations GID s1647 and GID g26133.

Appendix A: Table of Runs

Ra	Supercriticality	nz	nx	t_{therm}	$t_{\text{post BVP}}$	t_{avg}
$2.79 \cdot 10^3$	$10^{1/3}$	32	128	52.8	50	100
$6.01 \cdot 10^3$	$10^{2/3}$	32	128	77.6	50	100
$1.30 \cdot 10^4$	10^1	32	128	114	50	100
$2.79 \cdot 10^4$	$10^{1+1/3}$	32	128	167	50	100
$6.01 \cdot 10^4$	$10^{1+2/3}$	32	128	245	50	100
$1.30 \cdot 10^5$	10^2	64	256	360	100	100
$2.79 \cdot 10^5$	$10^{2+1/3}$	64	256	528	100	100
$6.01 \cdot 10^5$	$10^{2+2/3}$	64	256	776	100	100
$1.30 \cdot 10^6$	10^3	128	512	$1.14 \cdot 10^3$	100	200
$2.79 \cdot 10^6$	$10^{3+1/3}$	128	512	$1.67 \cdot 10^3$	200	200
$6.01 \cdot 10^6$	$10^{3+2/3}$	256	1024	$2.45 \cdot 10^3$	200	200
$1.30 \cdot 10^7$	10^4	256	1024	$3.60 \cdot 10^3$	200	200
$2.79 \cdot 10^7$	$10^{4+1/3}$	256	1024	$5.28 \cdot 10^3$	200	200
$6.01 \cdot 10^7$	$10^{4+2/3}$	256	1024	$7.76 \cdot 10^3$	200	200
$1.30 \cdot 10^8$	10^5	512	2048	$1.14 \cdot 10^4$	500	500
$2.79 \cdot 10^8$	$10^{5+1/3}$	512	2048	$1.67 \cdot 10^4$	500	500
$6.01 \cdot 10^8$	$10^{5+2/3}$	512	2048	$2.45 \cdot 10^4$	500	500
$1.30 \cdot 10^9$	10^6	1024	4096	$3.60 \cdot 10^4$	500	500

[1] M. Stix, "On the time scale of energy transport in the sun," Solar Physics **212**, 3–6 (2003).
[2] E. H. Anders and B. P. Brown, "Convective heat transport in stratified atmospheres at low and high Mach number," Physical Review Fluids **2**, 083501 (2017), arXiv:1611.06580 [physics.flu-dyn].
[3] A. Brandenburg, K. L. Chan, Å. Nordlund, and R. F. Stein, "Effect of the radiative background flux in convection," Astronomische Nachrichten **326**, 681–692 (2005), astro-ph/0508404.
[4] E. A. Spiegel and G. Veronis, "On the Boussinesq Approximation for a Compressible Fluid." Astrophys. J. **131**, 442 (1960).
[5] H. Johnston and C. R. Doering, "Comparison of Turbulent Thermal Convection between Conditions of Constant Temperature and Constant Flux," Phys. Rev. Lett. **102**, 064501 (2009), arXiv:0811.0401 [physics.flu-dyn].
[6] N. E. Hurlburt, J. Toomre, and J. M. Massaguer, "Two-dimensional compressible convection extending over multiple scale heights," Astrophys. J. **282**, 557–573 (1984).
[7] F. Cattaneo, N. H. Brummell, J. Toomre, A. Malagoli, and N. E. Hurlburt, "Turbulent compressible convection," Astrophys. J. **370**, 282–294 (1991).
[8] L. Korre, N. Brummell, and P. Garaud, "Weakly non-Boussinesq convection in a gaseous spherical shell," Phys. Rev. E **96**, 033104 (2017), arXiv:1704.00817 [physics.flu-dyn].
[9] K. Burns, G. Vasil, J. Oishi, D. Lecoanet, and B. Brown, "Dedalus: Flexible framework for spectrally solving differential equations," Astrophysics Source Code Library (2016), ascl:1603.015.
[10] U. M. Ascher, S. J. Ruuth, and R. J. Spiteri, "Implicit-explicit Runge-Kutta methods for time-dependent partial differential equations," Applied Numerical Mathematics **25**, 151–167 (1997).